Journal of Low Temperature Physics (2019) 197:357–378
https://doi.org/10.1007/s10909-019-02223-5

Magnetic, Magnetocaloric and Correlation with Critical Behavior in $Pr_{0.8}Sr_{0.2}MnO_3$ Compound Prepared via Solid-State Reaction

A. Ben Jazia Kharrat[1] · W. Boujelben[1]

Received: 25 May 2019 / Accepted: 24 July 2019 / Published online: 1 August 2019

Abstract
In this study, the critical behavior and magnetic and magnetocaloric properties in a polycrystalline $Pr_{0.8}Sr_{0.2}MnO_3$ sample synthesized by solid-state technique were investigated in detail. By analyzing the temperature and the field dependence of magnetization, we have demonstrated that this compound exhibits a clear second-order magnetic phase transition around the Curie temperature estimated at $T_C = 161$ K. Refined values of the critical exponents β, γ and δ determined by the modified Arrott plots, the critical isotherm and Kouvel–Fisher analysis show that our compound is described by the 3D Ising model. The reliability of these critical exponents was further confirmed using the universal scaling hypothesis. Under an applied magnetic field of 5 T, the calculated value of the maximum of the magnetic entropy change is estimated at 1.740 J K^{-1} kg^{-1} and the relative cooling power (RCP) turns out to be 134.46 J kg^{-1}. Moreover, the critical exponents were evaluated from RCP results which confirm the correlation between the critical behavior and magnetocaloric results in the $Pr_{0.8}Sr_{0.2}MnO_3$ compound.

Keywords Second-order phase transition · Critical behavior · Scaling hypothesis · Magnetocaloric effect

1 Introduction

Praseodymium perovskite materials with the general formula $Pr_{1-x}A_xMnO_3$ where A is an alkaline earth ion (such as Ca, Ba, Sr) still attract the interest of researchers owing to their important physical properties and their promising industrial applications. These properties can be controlled by defects, doping level, pressure, electric and magnetic

✉ A. Ben Jazia Kharrat
benjaziaaida@gmail.com

[1] Laboratoire de Physique des Matériaux, Faculté des Sciences de Sfax, Université de Sfax, B. P. 1171, 3000 Sfax, Tunisia

fields, etc. [1–4]. Moreover, from a fundamental point of view, the physical properties are governed by several parameters such as the Mn^{3+}/Mn^{4+} ratio, the average radius of the A-site and the cationic disorder in *A*- or *B*-site [1, 5].

Most attention was focused on manganite compounds exhibiting a large magnetocaloric effect (MCE) and colossal magnetoresistance (CMR) around the Curie temperature T_C such as $La_{0.6}Sr_{0.2}Na_{0.2}MnO_3$ [6] and $La_{0.7}Ca_{0.3-x}K_xMnO_3$ [7]. For magnetic refrigeration purpose, T_C should be around room temperature for domestic use [6]. However, materials with multifunctional properties are more interesting both fundamentally and technologically in addition to their environmental friendliness. Nevertheless, lead-based manganites may be useful as magnetic gas sensors [8]. Besides, cobalt-based materials exhibit good magnetotransport properties close to ambient temperature, giving rise to possible technological applications [9].

In this context, we have chosen the Pr-based manganites which are easy to elaborate, and in addition, their price is relatively low compared to other materials having the same characteristics.

Among these compounds, we have studied the $Pr_{0.8}Sr_{0.2}MnO_3$ compound prepared by solid-state reaction and quenched slowly in air [10] or quenched in water [11]. This compound shows high conductivity values, important dielectric constants and relatively low dielectric losses.

In order to pursue the investigation of this compound, we focus on studying the FM–PM phase transition around T_C. This transition is currently explained by the double-exchange theory proposed by Zener and the Jahn–Teller effect [12, 13]. Additionally, the critical behavior is studied on the basis of the critical exponents to understand whether they belong to long-range or short-range magnetic interactions. As well recognized, the critical behavior was studied for the first time in the framework of the mean field theory [14]. Actually, four different theoretical models can be used to explain the critical behavior of the majority of manganite materials, which are the mean field, 3D Ising, 3D Heisenberg [14] and the tricritical mean field [15] models. Both the 3D Ising model and the 3D Heisenberg model are simplified models of magnetism in materials. Furthermore, it has been demonstrated that the critical exponents in the majority of manganites belong to 3D Heisenberg or 3D Ising model describing short-range magnetic interaction between spins [16].

In this investigation, we report a detailed analysis of the magnetic and magnetocaloric properties of $Pr_{0.8}Sr_{0.2}MnO_3$ compound prepared by the conventional solid-state route. In addition, the critical exponent values were determined from the isothermal magnetic measurements by different methods and from magnetocaloric results.

2 Experimental Details

$Pr_{0.8}Sr_{0.2}MnO_3$ sample was successfully elaborated using the solid-state reaction technique [10]. Indeed, high-purity Pr_6O_{11}, $SrCO_3$ and MnO_2 precursors were at first well mixed in an agate mortar for 2 h and then heated at 1000 °C in air. The obtained powder was pressed into a pellet and sintered at 1400 °C with intermediate regrinding and pelletizing. The final step consists of quenching the obtained pellet rapidly in air

at room temperature in order to avoid the lack of oxygen stoichiometry. Consequently, our sample is stoichiometric in oxygen [17, 18]. In addition, the Mn^{3+} and Mn^{4+} contents were checked by chemical analysis. The Mn^{3+} and Mn^{4+} concentrations were, respectively, 79.89 and 20.11%.

Powder X-ray diffraction, at room temperature, was checked using CuKα radiation ($\lambda_{K\alpha} = 1.54056$ Å) and collected in the 2θ range 15°–100°. The obtained data, analyzed by means of the Rietveld method using the FullProf software [19], demonstrated that our material crystallizes in the orthorhombic system with *Pnma* space group and the lattice parameters are $a = 5.481(7)$ Å, $b = 7.734(8)$ Å and $c = 5.505(9)$ Å [10]. Additionally, the crystallite size obtained from XRD and the grain size obtained from SEM analysis are, respectively, 120 nm and 35 μm [10]. The magnetic measurements were taken by means of a cryogenic vibrating sample magnetometer operating between 5 and 350 K with an applied magnetic field $\mu_0 H$ up to 7 T. The obtained isothermals $M(\mu_0 H, T)$ were corrected by a demagnetization factor determined by a standard method on the basis of low-field magnetization measurements at low temperatures [20].

3 Results and Discussion

3.1 Magnetic Properties

Figure 1 illustrates the recorded magnetization temperature dependence $M(T)$ of the $Pr_{0.8}Sr_{0.2}MnO_3$ compound (noted PS1) under an applied magnetic field of $\mu_0 H = 0.05$ T. As can be observed, this sample displays a transition from paramagnetic (PM) to ferromagnetic (FM) state with the decrease in temperature. The Curie temperature T_C, corresponding to the minimum of the dM/dT curve, shown in the same figure, is determined to be 161 K. This value is close to that obtained by *B*. Christopher et al. estimated at 161.4 K [21] and determined in our previous work ($T_C = 162$ K) using a sample prepared also by the solid-state reaction but quenched in water [11]. On the other hand, Martin et al. [22] reported a transition temperature estimated at 150 K using the solid-state reaction. Let us also note that an important T_C value (210 K) is recorded for the same sample prepared using the sol–gel method [16].

Bourouina et al. [23] and Hueso et al. [24] have demonstrated that the decrease in T_C is correlated to the decrease in the grain size, which is explained in the first paper by the formation of nanostructured subgrains and in the second work by the formation of a non-magnetic layer whose origin is the existence of some non-crystallized regions which is more important as the grain size is smaller. On the other side, Zhang et al. [25] found that T_C decreases with the increase in grain size. They supposed that the contradiction could be attributed to the different doping levels.

A decrease in the Curie temperature T_C can be attributed also to the weakening of the double-exchange mechanism due to the decrease in the bandwidth W describing the overlap between the manganese and oxygen orbitals [16]. Many other factors can govern the T_C value such as the ionic radius of the A-site [26, 27], the increase of the Mn^{4+} ions [28], the disorder effect [29] and the preparation method [11, 16].

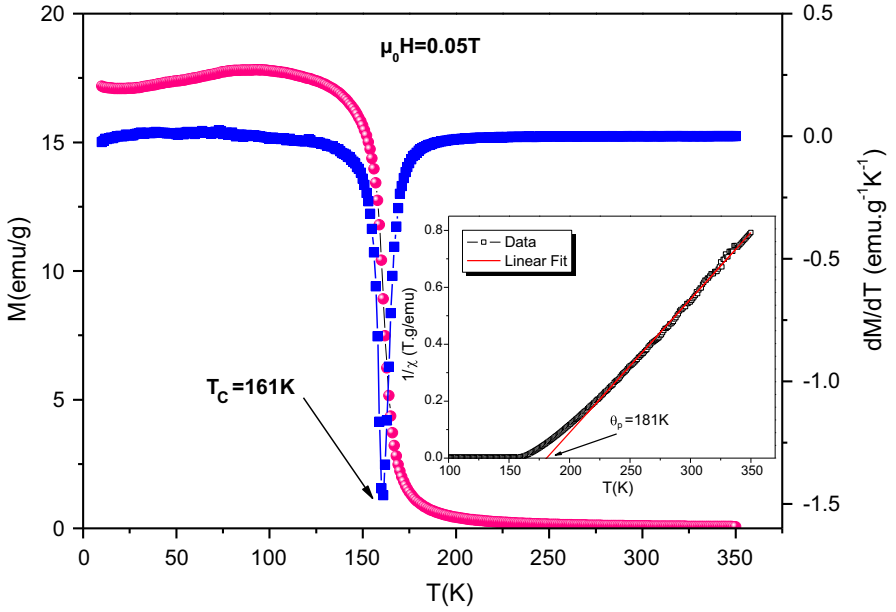

Fig. 1 Temperature dependence of the magnetization measured under an applied field of 0.05 T and the evolution of dM/dT (T) to determine T_C. The inset shows the inverse susceptibility versus temperature plot for $Pr_{0.8}Sr_{0.2}MnO_3$ compound (Color figure online)

The temperature dependence of the inverse susceptibility $1/\chi$ in the paramagnetic region is reported in the inset of Fig. 1. This curve follows the Curie–Weiss law given by:

$$\chi^{-1} = (T - \theta_W)/C \tag{1}$$

where θ_W and C are the Weiss temperature and the Curie constant, respectively. These parameters were determined from the linear fit of $\chi^{-1}(T)$ in the paramagnetic region. The Curie constant C is calculated theoretically using the formula:

$$C = \frac{\mu_0 \left(\mu_{\text{eff}}^{\text{exp}}\right)^2}{3k_B} \tag{2}$$

The permeability μ_0 and the Boltzmann constant k_B are equal to $4\pi\,10^{-7}$ H m^{-1} and 1.3810^{-23} J K^{-1}, respectively. Then, the experimental paramagnetic moment can be determined from relation (2). However, the theoretical value of the effective moment $\mu_{\text{eff}}^{\text{th}}$ is calculated from the following relation:

$$\left(\mu_{\text{eff}}^{\text{th}}\right)^2 = 0.8\left[\mu_{\text{eff}}^{\text{th}}\left(\text{Pr}^{3+}\right)\right]^2 + 0.8\left[\mu_{\text{eff}}^{\text{th}}\left(\text{Mn}^{3+}\right)\right]^2 + 0.2\left[\mu_{\text{eff}}^{\text{th}}\left(\text{Mn}^{4+}\right)\right]^2 \tag{3}$$

In this relation, the magnetic moments of Pr^{3+}, Mn^{3+} and Mn^{4+} ions are, respectively, 3.58, 4.9 and 3.87μ_B. The obtained values of $\mu_{\text{eff}}^{\text{exp}}$ and $\mu_{\text{eff}}^{\text{th}}$ are 6.418 and 5.697

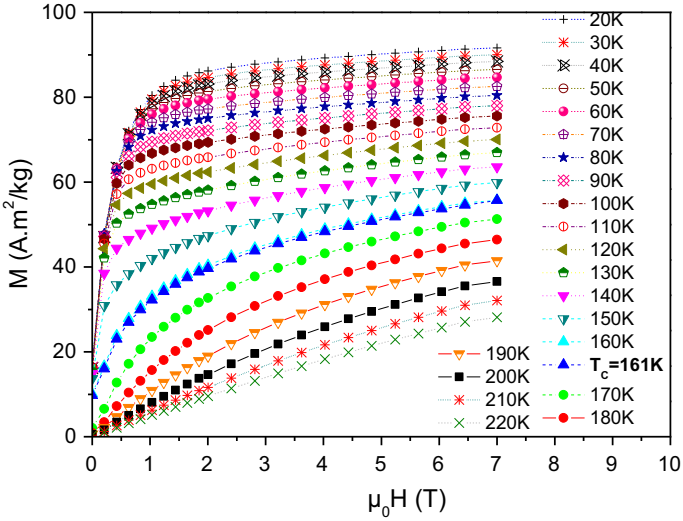

Fig. 2 Isothermal magnetization curves for $Pr_{0.8}Sr_{0.2}MnO_3$ sample (Color figure online)

μ_B, respectively. We can see that μ_{eff}^{exp} is larger than the expected theoretical one calculated from relation (3) suggesting the presence of a short-range magnetic order that can be attributed to the persistence of ferromagnetic correlations in the paramagnetic region [11]. Additionally, the obtained positive θ_W value (181 K) confirms the dominance of the interactions between Mn^{3+} and Mn^{4+} FM clusters.

It is worth noticing that this value of μ_{eff}^{exp} is lower than that obtained with the same sample prepared by the solid–solid reaction and quenched in water (8.036 μ_B) or by sol–gel route (7.687 μ_B) [11, 16]. These samples will be noted PS2 and PS3, respectively. In these samples, the ferromagnetic correlations in the paramagnetic region seem to be stronger.

Figure 2 shows the variation of the isothermal magnetization versus the applied magnetic field $M(\mu_0 H)$ for our $Pr_{0.8}Sr_{0.2}MnO_3$ studied sample. At low temperature and applied magnetic field values, we can remark that magnetization increases sharply with the increase of $\mu_0 H$ which characterizes the presence of a ferromagnetic behavior. Far from T_C (around 200 K), the magnetization increases linearly with the increase in applied magnetic field which is the signature of a PM state.

So as to analyze the order of the magnetic transition, we have determined the Arrott plots showing the evolution of M^2 versus $\mu_0 H/M$. These curves are depicted in Fig. 3. As can be seen, the positive slopes of the Arrott plots for $Pr_{0.8}Sr_{0.2}MnO_3$ compound confirm a second-order magnetic PM–FM transition according to Banerjee criterion [30].

3.2 Critical Behavior

The modified Arrott–Noakes plots, obtained from the isothermal M(μ_0H) results measured around T_C (see Fig. 4a), were determined using the trial critical exponents β

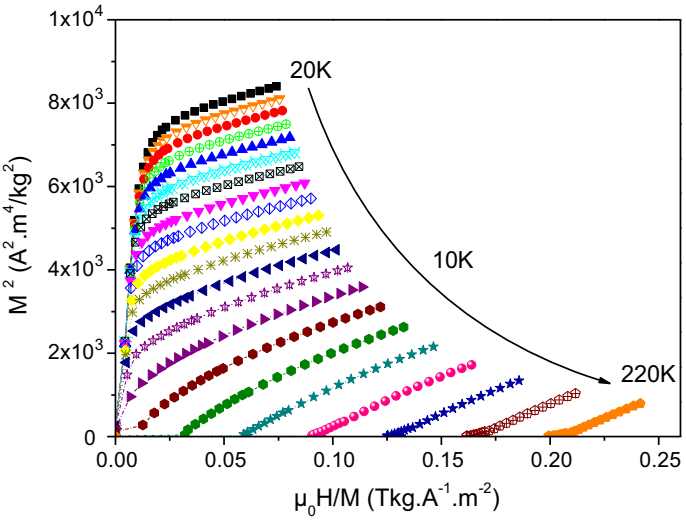

Fig. 3 Modified Arrott plots (M^2 versus μ_0H/M at different temperatures) for $Pr_{0.8}Sr_{0.2}MnO_3$ compound (Color figure online)

and γ of the four theoretical models: the mean field, the tricritical mean field, the 3D Ising and the 3D Heisenberg one. The β and γ values obey the following relation [31]:

$$\left(\frac{\mu_0 H}{M}\right)^{\frac{1}{\gamma}} = K_0\varepsilon + K_1(M)^{\frac{1}{\beta}} \tag{4}$$

In this formula, K_0 and K_1 are considered as constants, and $\varepsilon = (T - T_C)/T_C$ is the reduced temperature.

Figure 4b–e displays the plots showing the modified Arrott plots obtained for the $Pr_{0.8}Sr_{0.2}MnO_3$ compound. As clearly observed, in the high-magnetic-field region, all these models yield almost a set of quasi-straight lines, but the selected model is that which gives straight parallel lines in the high-field region. A comparison of these models can be evaluated by calculating the relative slopes (RS) determined at high magnetic fields using the following relation:

$$\mathrm{RS} = \frac{S(T)}{S(T = T_C)} \tag{5}$$

where $S(T)$ and $S(T = T_C)$ are the slopes at a temperature close to the Curie temperature and the slope at T_C, respectively. The best model can be chosen when the RS values around T_C are close to unity regardless of the temperature.

Figure 5 illustrates the temperature evolution of the RS values relative to the $Pr_{0.8}Sr_{0.2}MnO_3$ compound. A simple analysis of the results shows that the behavior of the studied sample is consistent with the 3D Ising model where spins can acquire the values ± 1 on each site of the lattice. This result goes in good agreement with that obtained with the PS2 and the $Pr_{0.8-x}Bi_xSr_{0.2}MnO_3$ ($x = 0.05$ and 0.1) com-

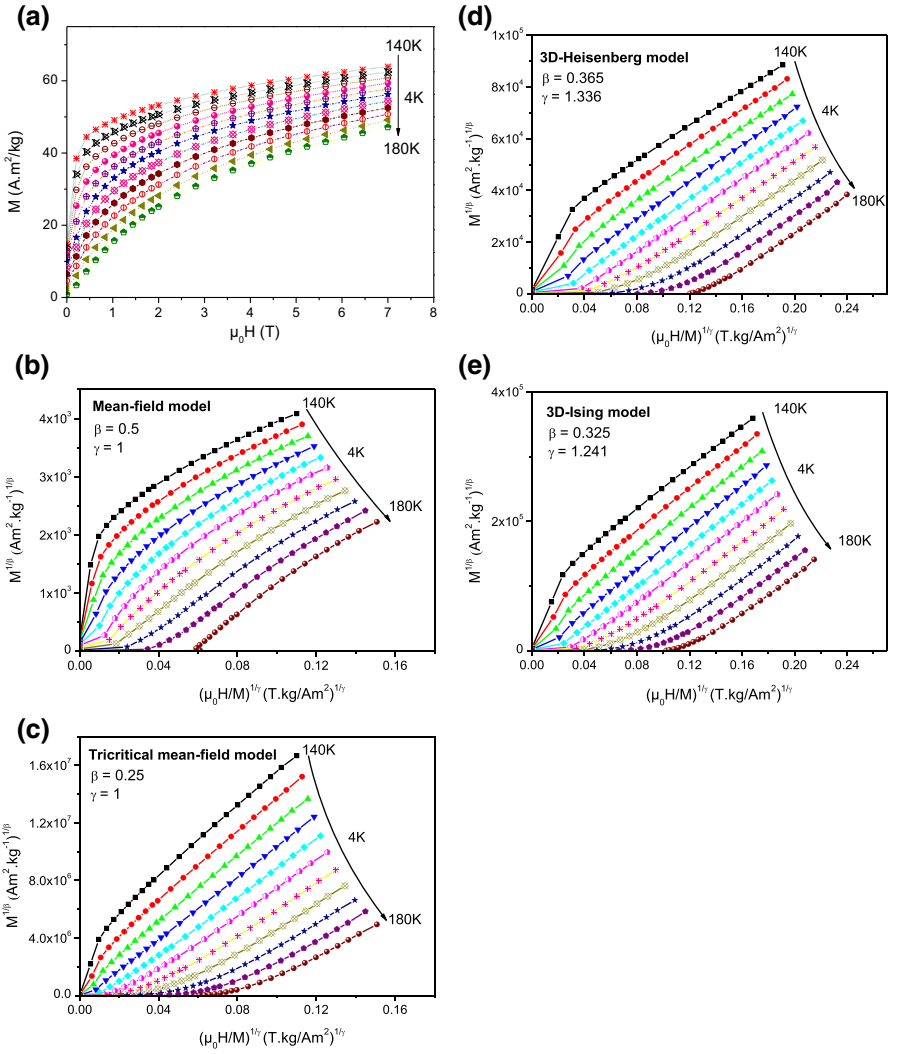

Fig. 4 **a** Magnetic field dependence of the magnetization determined at temperatures around T_C, **b–e** modified Arrott plots for $Pr_{0.8}Sr_{0.2}MnO_3$ sample (Color figure online)

pounds [11, 16]. Contrariwise, the magnetic phase transition of the PS2 sample can be described by the tricritical mean field model.

As a comparison, the transition behavior of $Pr_{0.5-x}Gd_xSr_{0.5}MnO_3$ ($x = 0$; 0.05 and 0.1) [5] and $La_{0.67}Sr_{0.33}MnO_{3.01}$ [32] compounds is in good agreement with the mean field model, implying the existence of long-range magnetic interaction.

Using the obtained critical exponents relative to the 3D Ising model as trial values, we have reported in Fig. 6a the temperature evolution of the spontaneous magnetization $M_{SP}(T)$ and the inverse of susceptibility $\chi^{-1}(T)$ for our compound. Our target is to

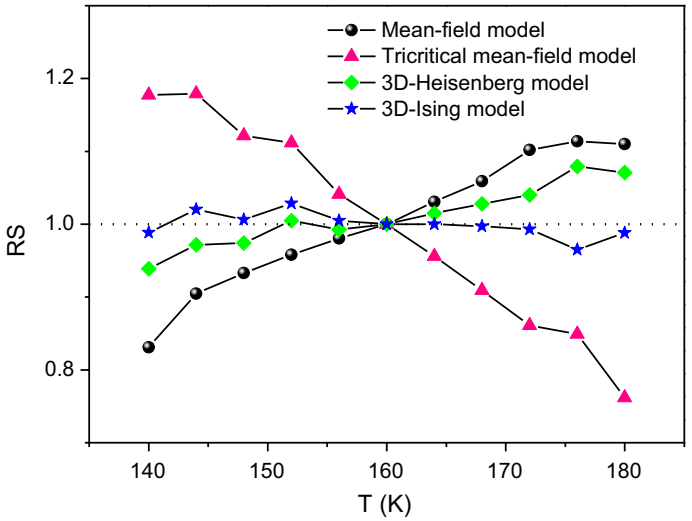

Fig. 5 Temperature evolution of the relative slope RS using several models for $Pr_{0.8}Sr_{0.2}MnO_3$ compound (Color figure online)

determine more precisely the γ and β values describing the PM behavior below T_C and the FM behavior above T_C.

Currently, the critical exponents β, γ and δ can be expressed using the following equations [33]:

$$M_{sp}(T) = M_{sp}(0)(-\varepsilon)^{\beta} \qquad T < T_C \tag{6}$$

$$\chi^{-1}(T) = \chi^{-1}(0)(\varepsilon)^{\gamma} \qquad T > T_C \tag{7}$$

and

$$M(\mu_0 H) = A(\mu_0 H)^{1/\delta} \qquad T = T_C \tag{8}$$

In these relations, $M_{SP}(0)$ and $\chi^{-1}(0)$ denote, respectively, the spontaneous magnetization and the inverse of susceptibility determined at 0 K, whereas A is a critical amplitude. The power-law fitting of $M_{SP}(T)$ and $1/\chi(T)$ using relations (3) and (4) is also shown in Fig. 6a. The obtained values of β, γ and the accurate average value of T_C are 0.318(3), 1.260(7) and 161.904(5), respectively.

Additionally, the third critical exponent δ can be obtained from the critical isotherm M(161 K, $\mu_0 H$) curve reported in Fig. 6b in linear scale and with Ln(M) versus Ln($\mu_0 H$) scale in the inset. In the high-magnetic-field region and according to relation (5), the Ln(M)–Ln($\mu_0 H$) plots show straight lines with slopes of $1/\delta$. The estimated value of δ is 4.831(3). The δ value can be also calculated using the Widom scaling relation given by [34]:

$$\delta = 1 + \gamma/\beta \tag{9}$$

Table 1 Critical exponents of the $Pr_{0.8}Sr_{0.2}MnO_3$ sample and of other materials listed as comparison

Compound	Technique	T_C (K) (average)	β	γ	δ	Refs.
Mean field model	Theory		0.5	1	3	[14]
Tricritical mean field model	Theory		0.25	1	5	[15]
3D Heisenberg model	Theory		0.365	1.336	4.8	[14]
3D Ising model	Theory		0.325	1.24	4.82	[14]
$Pr_{0.8}Sr_{0.2}MnO_3$ (solid–solid)	MAP	161.905	0.318(3)	1.260(7)		This work
	KF	161.715	0.326(6)	1.246(8)		
	CI(exp)				4.831(3)	
	CI(cal)				4.960(7)	
PS2	KF	162.251	0.335(1)	1.239(0)	4.489	[11]
PS3	KF	210.828	0.260(4)	0.993(2)	4.81	[16]
$Pr_{0.55}Sr_{0.45}MnO_3$	KF	290	0.462	1.033	4.749	[37]
$Pr_{0.67}Ba_{0.33}MnO_3$	KF	201	0.246	1.03	5.069	[38]

Using relation (6) together with the values of β and γ obtained previously from MAP, the calculated value of δ is 4.960(7), which is in good agreement with that calculated from the critical isotherm at $T_C = 161$ K. All obtained values are gathered in Table 1. (CI indicates the critical isotherm.) A comparison between the obtained critical exponents and theoretical ones confirms that the 3D Ising model is the most satisfying model for describing magnetic interactions around the Curie temperature.

An additional method to determine accurately the critical exponents as well as the Curie temperature is the Kouvel–Fisher method [35] based on the following relations:

$$\chi_0^{-1}(T) \cdot \left[\frac{\mathrm{d}\chi_0^{-1}(T)}{\mathrm{d}T}\right]^{-1} = \frac{T - T_C}{\gamma} \tag{10}$$

$$M_S(T) \cdot \left[\frac{\mathrm{d}M_S(T)}{\mathrm{d}T}\right]^{-1} = \frac{T - T_C}{\beta} \tag{11}$$

From a physical point of view, the parameter β describes how the ordered magnetic moment grows below the Curie temperature, while the critical exponent γ characterizes the divergence of χ values at temperatures above T_C [36].

The evaluation of the critical exponents γ and β requires the plotting of the $\chi_0^{-1}(T) \cdot \left[\frac{\mathrm{d}\chi_0^{-1}(T)}{\mathrm{d}T}\right]^{-1}$ and $M_S(T) \cdot \left[\frac{\mathrm{d}M_S(T)}{\mathrm{d}T}\right]^{-1}$ curves. Figure 6c depicts the fitting of these plots by a straight line using relations (7) and (8). The obtained slopes are, respectively, $1/\beta$ and $1/\gamma$. It is noticeable that the intercept of these curves with the axis temperature allows us to determine the Curie temperature. The results, with those of other materials as comparison [11, 16, 37, 38], are gathered in Table 1. It is worth noticing that the obtained values of the critical exponents and the Curie temperature

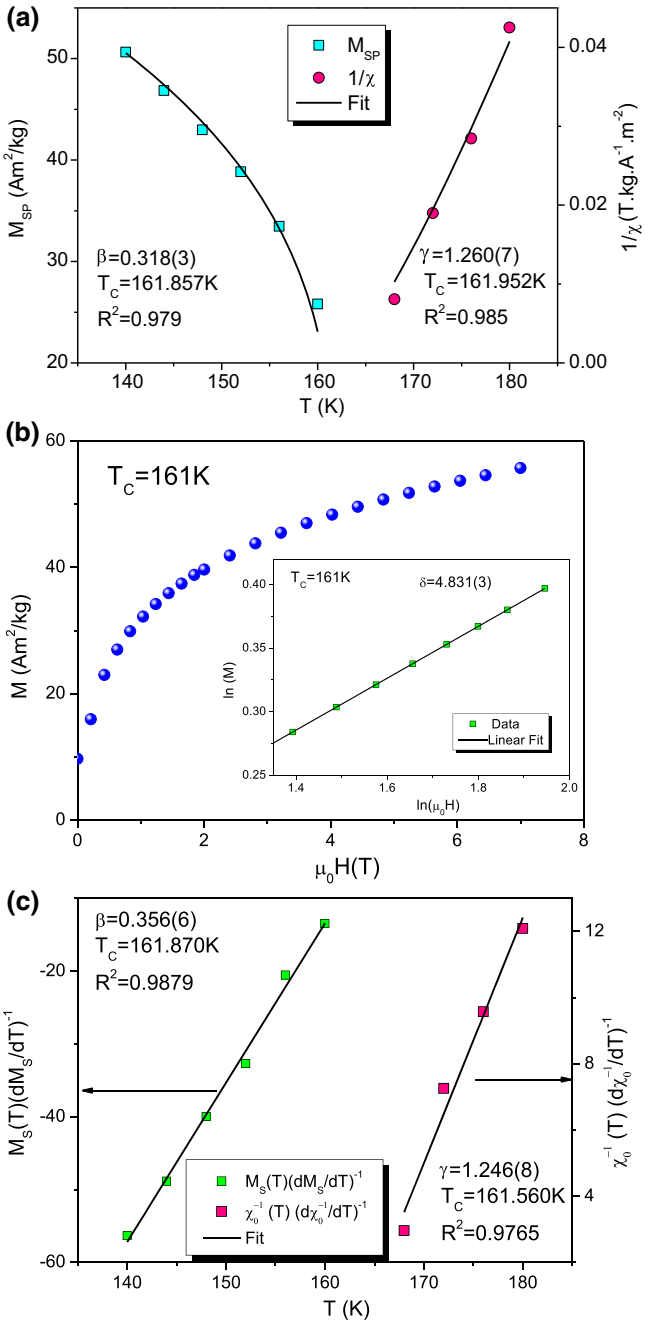

Fig. 6 **a** Temperature dependence of the spontaneous magnetization $M_S(T)$ and the inverse of initial susceptibility $\chi^{-1}(T)$, **b** isothermal magnetic plot at $T = T_C$. The inset shows the same plot for the high-field region using a logarithmic scale, **c** Kouvel–Fisher plots for the spontaneous magnetization $M_S(T)$ and the inverse of initial susceptibility $\chi^{-1}(T)$ as a function of temperature for $Pr_{0.8}Sr_{0.2}MnO_3$ compound (Color figure online)

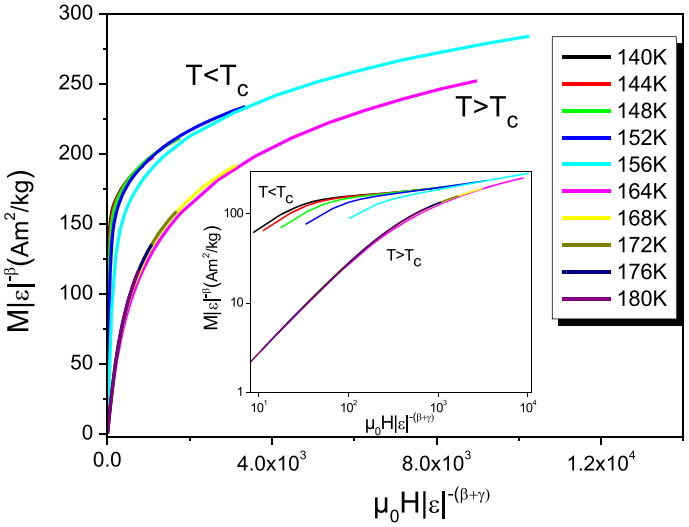

Fig. 7 Scaling plots indicating two universal curves below and above T_C for $Pr_{0.8}Sr_{0.2}MnO_3$ sample. The inset shows the same plot in a Ln–Ln scale (Color figure online)

show a good satisfaction with those obtained from modified Arrott plots (MAP) of the 3D Ising model. This suggests a short-range magnetic interaction.

The reliability of the critical exponents can be checked by scaling analysis. Indeed, according to this theory, the magnetization M and the applied magnetic field $\mu_0 H$ are related, around T_C, by [39]:

$$M(\mu_0 H, \varepsilon) = \varepsilon^{\beta} f_{\pm}\left(\frac{\mu_0 H}{\varepsilon^{\beta+\gamma}}\right) \tag{12}$$

In this formula, $f_{\pm}$ are regular functions: f_- below T_C ($\varepsilon < 0$) and f_+ above T_C ($\varepsilon > 0$). Using the critical exponents β and γ determined on the basis of the KF method, we have plotted in Fig. 7 the evolution of $M\,|\varepsilon|^{-\beta}$ as a function of $(\mu_0 H\,|\varepsilon|^{-\beta+\gamma})$ for our $Pr_{0.8}Sr_{0.2}MnO_3$ compound. As noticed, all obtained curves collapse into two different curves: the first one is for temperatures below T_C and the second for temperatures above T_C. Such a result highlights the accuracy of the critical exponents obtained in this study. In addition, the reliability of these critical values is outlined by the same curves plotted in a logarithmic scale (see the inset of Fig. 7).

3.3 Magnetocaloric Effect

Although the materials with second-order magnetic FM–PM phase transition show a lower magnetocaloric effect (MCE) as compared with materials with a first-order magnetic transition [32, 40], we have investigated the magnetocaloric effect in this compound in order to evaluate its efficiency using the magnetic results. Indeed, around the Curie temperature, the release of heat induces an important increase in the variation of the magnetic entropy. The magnetic entropy change ΔS_M versus temperature can be

calculated from the magnetization measurements as a function of the applied magnetic field $M(\mu_0 H)$ based on the Maxwell relation:

$$\Delta S_{\mathrm{M}}(T, \mu_0 H) = S_{\mathrm{M}}(T, \mu_0 H) - S_{\mathrm{M}}(T, 0) = \int_0^{\mu_0 H} \left(\frac{\partial M}{\partial T}\right)_{\mu_0 H} d(\mu_0 H) \tag{13}$$

ΔS_{M} can be obtained by integrating numerically in the given range of magnetic fields based on the set of isothermal magnetism $M(\mu_0 H)$ curves measured at different temperatures. The $\Delta S_{\mathrm{M}}(T)$ can also be estimated by the formula:

$$\Delta S_{\mathrm{M}}(T, \mu_0 H) = \sum_i \frac{M_{i+1}(T_{i+1}, \mu_0 H) - M_i(T_i, \mu_0 H)}{T_{i+1} - T_i} \Delta(\mu_0 H) \tag{14}$$

where M_i and M_{i+1} are the experimental magnetization data measured under the applied magnetic field μ_0H, at the temperatures T_i and T_{i+1}, respectively.

Figure 8a illustrates the evolution of the magnetic entropy change $(-\Delta S_{\mathrm{M}})$ with temperature and the external magnetic field. As shown, at fixed μ_0H, $(-\Delta S_{\mathrm{M}})$ increases and reaches a maximum noted $\left(-\Delta S_{\mathrm{M}}^{\mathrm{Max}}\right)$ at Curie temperature. Additionally, $\left(-\Delta S_{\mathrm{M}}^{\mathrm{Max}}\right)$ shifts toward higher temperatures indicating the reinforcement of the FM behavior following the application of the applied magnetic field. The maximum $\left(-\Delta S_{\mathrm{M}}^{\mathrm{Max}}\right)$ obtained is 1.740 J K^{-1} kg^{-1} under an applied magnetic field of 5 T. It is worth noticing that large magnetocaloric results can be obtained in perovskite manganites which may be attributed to the spin–lattice coupling during the ordering process [41].

In order to evaluate the magnetic cooling efficiency of the studied compound, we have calculated the relative cooling power (RCP) given by [42]:

$$\mathrm{RCP} = -\Delta S_{\mathrm{M}}^{\mathrm{Max}}(T, \mu_0 H) \times \Delta T_{\mathrm{FWHM}} \tag{15}$$

where ΔT_{FWHM} is the full width at half maximum which corresponds to the curve giving the temperature dependence of $\left(-\Delta S_{\mathrm{M}}^{\mathrm{Max}}\right)$ shown in Fig. 8a. We summarize in Table 2 the values of $\left(-\Delta S_{\mathrm{M}}^{\mathrm{Max}}\right)$, ΔT_{FWHM} and RCP for $Pr_{0.8}Sr_{0.2}MnO_3$ and other materials as a comparison [43–49]. As seen, the RCP results may be enhanced by the application of stronger magnetic field confirming the field dependence of this parameter.

Furthermore, we have shown in Fig. 8b the comparison between RCP values obtained for the three compounds PS1, PS2 and PS3 and the RCP of gadolinium considered as the best candidate for magnetic refrigeration [49]. As seen, the RCP values of the PS1, PS2 and PS3 compounds represent 32.8, 76.1 and 48.3% of that of Gd. Although our compound gives the lowest RCP, the ΔT_{FWHM} is the highest one which broadens the use of this sample in a wide range of temperature around T_{C}.

As well recognized, the magnetic field dependence of $\left(-\Delta S_{\mathrm{M}}^{\mathrm{Max}}\right)$ can be estimated, around the Curie temperature and for materials with second-order transition by the universal relation [50]:

$$\left(-\Delta S_{\mathrm{M}}^{\mathrm{Max}}\right) = A(\mu_0 H)^n \tag{16}$$

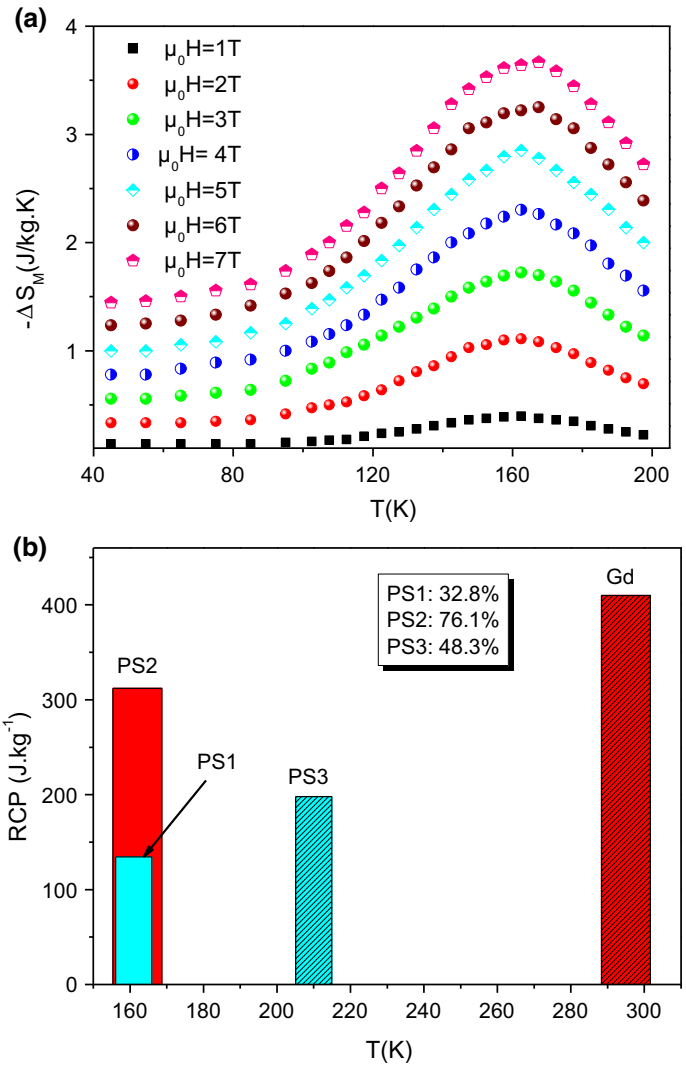

Fig. 8 **a** Temperature evolution of the magnetic entropy change as for several applied magnetic fields values, **b** for the $Pr_{0.8}Sr_{0.2}MnO_3$ sample (Color figure online)

In this expression, n is a critical exponent depending on the magnetic state of the studied compound and A is a proportionality constant.

The magnetic field dependence of the maximum entropy change $\left(-\Delta S_{\mathrm{M}}^{\mathrm{Max}}\right)$ for our compound is displayed in Fig. 9a. The fit of this curve with good accuracy, using relation (16), gives $n = 0.891$, which is higher than that obtained for FM materials in the mean field theory where n is equal to 2/3 at T_{C} [51]. This result confirms the appearance of a short-range FM order in our sample, which can be attributed to the persistence of local magnetic clusters above T_{C}.

Table 2 ($-\Delta S_{max}$), RCP and ΔT_{FWHM} values calculated at different applied magnetic fields for $Pr_{0.8}Sr_{0.2}MnO_3$ sample and values relative to other compounds as comparison

	$\mu_0 H$ (T)	$-\Delta S_{Max}$ (J K^{-1} kg^{-1})	ΔT_{FHWM} (T)	RCP (J kg^{-1})	Refs.
$Pr_{0.8}Sr_{0.2}MnO_3$ (solid–solid)	1	0.245	62.634	15.35	This work
	2	0.740	70.669	52.30	
	3	1.107	79.689	88.22	
	4	1.425	76.323	108.76	
	5	1.740	77.273	134.46	
	6	1.970	77.730	154.13	
	7	2.182	77.326	168.73	
$Pr_{0.8}Sr_{0.2}MnO_3$	1	1.27	34.62	44.05	[11]
PS2	2	2.14	47.41	101.52	
	3	2.84	59.88	170.27	
	4	3.49	68.70	239.98	
	5	4.09	76.24	312.04	
$Pr_{0.8}Sr_{0.2}MnO_3$	1	1.12	22.77	25.50	[16]
PS3	2	2.81	26.63	74.83	
	3	3.95	30.52	120.55	
	4	4.79	33.83	162.05	
	5	5.41	36.59	197.95	
$Pr_{0.8}Pb_{0.2}MnO_3$	1.35	2.64	–	55	[43]
$La_{0.67}Ba_{0.22}Sr_{0.11}MnO_3$	5	2.75	–	290	[44]
$La_{0.8}Sr_{0.2}MnO_3$	5	3.77	–	259.78	[45]
$Pr_{0.6}Sr_{0.4}MnO_3$	2	1.55	–	62.11	[46]
$La_{0.8}Ca_{0.2}MnO_3$	1.5	5.5	–	72	[47]
$Gd_5Si_2Ge_2$	5	18.4	–	535	[48]
Gd	5	9.5		410	[49]

On the other hand, this parameter can be expressed locally by the formula [52]:

$$n(T, \mu_0 H) = \frac{d\,\mathrm{Ln}|\Delta S_M|}{d\,\mathrm{Ln}(\mu_0 H)} \tag{17}$$

The evolution of $n(T, \mu_0 H)$ for the $Pr_{0.8}Sr_{0.2}MnO_3$ compound is displayed in Fig. 9b. As clearly seen, n decreases, and then, it shows a minimum at Curie temperature. At low and high temperatures and as suggested by Franco et al. [53], the asymptotic values of n are 1 and 2, respectively. This behavior is typical in manganites. It shows the non-magnetic homogeneity of our compound, in particular around T_C.

Using the magnetocaloric results plotted in Fig. 8a, we have constructed, according to Franco et al. [54], a phenomenological universal curve based on the following relations:

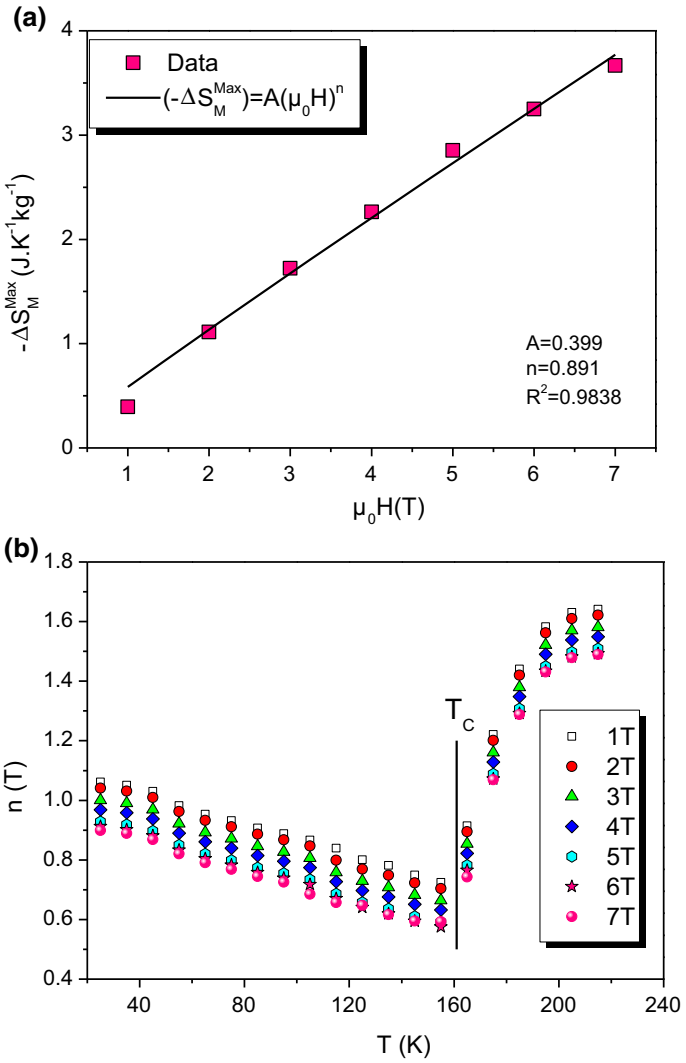

Fig. 9 **a** Temperature evolution of the magnetic entropy change for several applied magnetic fields, **b** comparison between RCP values for PS1, PS2, PS3 and the RCP of gadolinium (Color figure online)

$$\theta = \begin{cases} -\frac{(T-T_C)}{(T_1-T_C)}, & T \leq T_C \\ \frac{(T-T_C)}{(T_2-T_C)}, & T > T_C \end{cases} \tag{18}$$

At fixed $\mu_0 H$, $\Delta S_M(T)$ is normalized using its peak entropy change $\left(-\Delta S_M^{Max}\right)$ and the temperature is rescaled below and above the Curie temperature T_C.

In relation (18), θ is the rescaled temperature and T_1 and T_2 are the temperatures of the two reference points obtained for $S_M = \left(-\Delta S_M^{Max}\right)/2$. The evolution of the

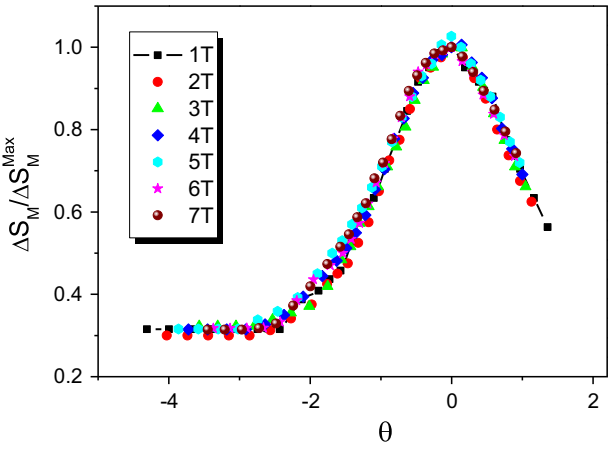

Fig. 10 Normalized ($-\Delta S_M$) data versus rescaled temperature for $Pr_{0.8}Sr_{0.2}MnO_3$ compound (Color figure online)

normalized entropy change as a function of θ for different applied magnetic fields is gathered in Fig. 10. It is well illustrated by analyzing this figure that all experimental data collapse into one universal curve confirming the reversible behavior of the second-order magnetic phase transition for our studied compound.

3.4 Correlation Between Critical Exponents and Magnetocaloric Results

Using the values of RCP calculated at different applied magnetic fields and the exponent n calculated from relation (16), we can estimate the isothermal magnetic susceptibility exponent γ, the spontaneous magnetization exponent β and the critical isotherm exponent δ. As we have mentioned previously, these critical exponents characterize the magnetic transition around T_C.

At the Curie temperature, the n exponent value can be determined using the relation proposed by Franco et al. [51]:

$$n(T_C) = 1 + \frac{1}{\delta}\left(1 - \frac{1}{\beta}\right) \tag{19}$$

We have calculated this value using the critical exponents β and δ calculated with the KF theory and the Widom scaling relation, respectively. We have obtained $n = 0.572$ which is not far from that obtained using the 3D Ising model (0.569) confirming the validity of this model to describe the magnetic interactions in the vicinity of T_C.

Furthermore, the exponent calculated previously can be determined for $T = T_C$, using the relation [55]:

$$n(T_C) = 1 + (\beta - 1)/(\beta + \gamma) \tag{20}$$

The magnetic field dependence of RCP can be given by the following expression [54]:

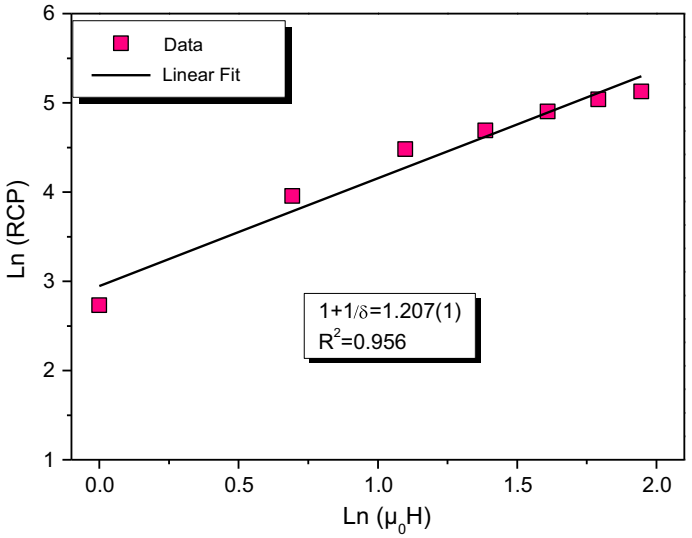

Fig. 11 Evolution of Ln(RCP) versus Ln($\mu_0 H$) to determine the critical exponent δ (Color figure online)

$$\mathrm{RCP} = (\mu_0 H)^{1+1/\delta} \tag{21}$$

In this relation, α is a constant.

In Fig. 11, we have plotted the evolution of Ln(RCP) versus Ln($\mu_0 H$) for our compound. The slope of this curve (1 + 1/δ) gives the critical exponent $\delta = 4.828$. Then, β and γ values can be calculated using relations (19) and (20). We have obtained $\beta = 0.326$ and $\gamma = 1.249$ confirming the correlation between the critical behavior and the magnetocaloric results for $Pr_{0.8}Sr_{0.2}MnO_3$ compound.

Another scaling equation is also proposed by Franco et al. [56] where the magnetic entropy change is given by:

$$-\Delta S_{\mathrm{M}}(T, \mu_0 H)/a_{\mathrm{M}} = A_0(\mu_0 H)^{\frac{2\beta+\gamma-1}{\beta+\gamma}} S\left[\frac{\mathrm{Tr}}{(\mu_0 H)^{\frac{1}{\beta+\gamma}}}\right] \tag{22}$$

where $\mathrm{Tr} = \frac{T_{\mathrm{C}}-T}{T_{\mathrm{C}}}$ is the reduced temperature and $a_{\mathrm{M}} = T_{\mathrm{C}}^{-1} A_0^{\delta+1} B$, being A_0 and B the critical amplitudes [43]. Figure 12 displays the evolution of $-\Delta S_{\mathrm{M}}(T, \mu_0 H)/(\mu_0 H)^{\frac{2\beta+\gamma-1}{\beta+\gamma}}$ versus $\mathrm{Tr} \cdot (\mu_0 H)^{-\frac{1}{\beta+\gamma}}$ relative to our studied sample. As shown, all experimental values collapse in a single curve, confirming that there is a good correlation between the magnetocaloric and the critical behavior for the $Pr_{0.8}Sr_{0.2}MnO_3$ compound.

This method offers the possibility to characterize new magnetic materials based on the universal curve. In addition, it allows the selection of the most efficient materials for magnetic refrigeration by extrapolating to fields and temperatures not available in the laboratory.

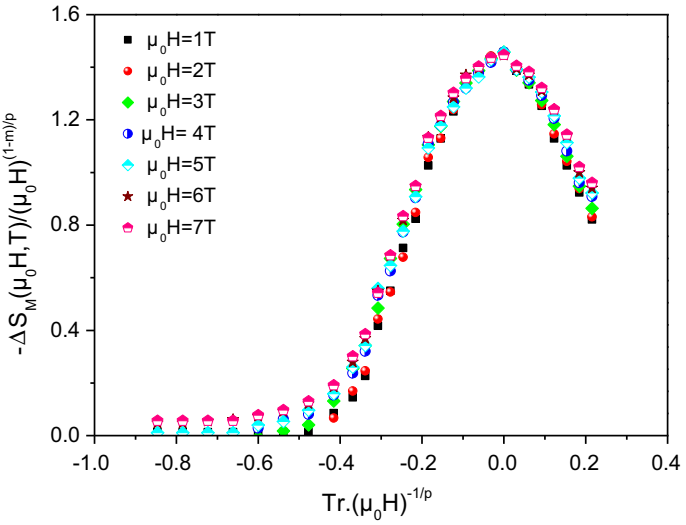

Fig. 12 Evolution of the scaled magnetic entropy change with scaled temperature using critical exponents for $Pr_{0.8}Sr_{0.2}MnO_3$ compound (Color figure online)

4 Conclusion

The polycrystalline $Pr_{0.8}Sr_{0.2}MnO_3$ compound was synthesized by the solid-state reaction.

An investigation of the critical behavior and magnetic properties was presented in detail. The Arrott plots show a second-order FM–PM transition. Using various techniques such as modified Arrott plots, the critical isotherm method and Kouvel–Fischer analysis, we have demonstrated that the magnetic phase transition is described by the 3D Ising model suggesting short-range magnetic exchange interactions. The validity of the obtained critical exponents is confirmed by scaling analysis. Furthermore, a detailed analysis of $(-\Delta S_M)$ and RCP allows us to determine the range of temperature where the compound is more efficient. The magnetic entropy change follows the universal law confirming the second-order PM–FM transition. The critical exponents were also determined through magnetocaloric results. A good agreement was obtained between the two methods confirming the correlation between the critical behavior and the magnetocaloric properties of this compound.

Acknowledgements This work has been supported by the Tunisian Ministry of Higher Education and Scientific Research.

References

1. A.B.J. Kharrat, M. Bourouina, N. Moutia, K. Khirouni, W. Boujelben, Gd doping effect on impedance spectroscopy properties of sol–gel prepared $Pr_{0.5-x}Gd_xSr_{0.5}MnO_3$ ($0 \le x \le 0.3$) perovskites. J. Alloys Compd. **741**, 723–733 (2018)

2. V. Markovich, I. Fita, R. Puzniak, A. Wisniewski, K. Suzuki, J.W. Cochrane, Y. Yuzhelevskii, Y.M. Mukovskii, G. Gorodetsky, Pressure effects on the magnetic and transport properties of $Pr_{1-x}Sr_xMnO_3$ crystals near the percolation threshold. Phys. Rev. B **71**, 224409 (2005)
3. H.E. Sekrafi, A.B.J. Kharrat, M.A. Wederni, N. Chniba-Boudjada, K. Khirouni, W. Boujelben, Impact of low titanium concentration on the structural, electrical and dielectric properties of $Pr_{0.75}Bi_{0.05}Sr_{0.1}Ba_{0.1}Mn_{1-x}Ti_xO_3$ ($x = 0{,}0.04$) compounds. J. Mater. Sci. Mater. Electron. **30**, 876 (2019)
4. D.C. Krishna, P.V. Reddy, Magnetic transport behavior of nano-crystalline $Pr_{0.67}A_{0.33}MnO_3$ ($A =$ Ca, Sr, Pb and Ba) manganites. J. Alloys Compd. **479**, 661–669 (2009)
5. A.B.J. Kharrat, M. Bourouina, N. Chniba-Boudjada, W. Boujelben, Critical behaviour of $Pr_{0.5-x}Gd_xSr_{0.5}MnO_3$ ($0 \leq x \leq 0.1$) manganite compounds: correlation between experimental and theoretical considerations. Solid State Sci. **87**, 27 (2019)
6. S. Hcini, R. Charguia, A. Dhahri, M.L. Bouazizi, Bouazizi, structural analysis, magnetocaloric effect, and critical exponents for $La_{0.6}Sr_{0.2}Na_{0.2}MnO_3$ anganite. J. Supercond. Nov. Magn. (2019). https://doi.org/10.1007/s10948-018-988-x
7. L. Li, H. Zhang, X. Liu, P. Sun, C. Wang, X. Wang, B. Li, G. Liang, Q. Chen, Structure and electromagnetic properties of $La_{0.7}Ca_{0.3-x}K_xMnO_3$ polycrystalline ceramics. Ceram. Int. **45**, 10558–10564 (2019)
8. A. Rinkevich, A. Nosov, M.B. Rigmant, V.G. Vasil'ev, E.V. Vladimirova, Magnetic-field sensors based on lead-doped lanthanum manganites. Russ. J. Nondestr. Test. **42**, 516–524 (2006)
9. L.M. Rodriguez-Martinez, J.P. Attfield, Cation disorder and size effects in magnetoresistive manganese oxide perovskites. Phys. Rev. B **54**, R15622–R15625 (1996)
10. A.B.J. Kharrat, N. Moutia, K. Khirouni, W. Boujelben, Investigation of electrical behavior and dielectric properties in polycristalline $Pr_{0.8}Sr_{0.2}MnO_3$ manganite perovskite. Mater. Res. Bull. **105**, 75–83 (2018)
11. A.B.J. Kharrat, K. Khirouni, W. Boujelben, Structural, magnetic, magnetocaloric and impedance spectroscopy analysis of $Pr_{0.8}Sr_{0.2}MnO_3$ manganite prepared by modified solid-state route. Phys. Lett. A **382**, 3435–3448 (2018)
12. C. Zener, Interaction between the d-shells in the transition metals. II. Ferromagnetic compounds of manganese with perovskite structure. Phys. Rev. **82**, 403–405 (1951)
13. F. He, Z. Mao, L. Tang, J. Zhang, X. Chen, The Jahn–Teller distortion influenced ferromagnetic order in $Pr_{1-x}La_xMnO_3$. Solid State Commun. **274**, 21–26 (2018)
14. S.N. Kaul, Static critical phenomena in ferromagnets with quenched disorder. J. Magn. Magn. Mater. **53**, 5–53 (1985)
15. K. Huang, *Statistical Mechanics*, 2nd edn. (Wiley, New York, 1987)
16. A.B.J. Kharrat, E.K. Hlil, W. Boujelben, Tuning the magnetic and magnetotransport properties of $Pr_{0.8}Sr_{0.2}MnO_3$ manganites through Bi-doping. Mater. Res. Express **5**, 126107 (2018)
17. H.E. Sekrafi, A.B.J. Kharrat, M.A. Wederni, K. Khirouni, N. Chniba-Boudjada, W. Boujelben, Structural, electrical, dielectric properties and conduction mechanism of sol–gel prepared $Pr_{0.75}Bi_{0.05}Sr_{0.1}Ba_{0.1}Mn_{0.98}Ti_{0.02}O_3$ compound. Mater. Res. Bull. **111**, 329–337 (2019)
18. S.V. Trukhanova, I.O. Troyanchuka, N.V. Pushkareva, H. Szymczakb, The influence of oxygen deficiency on the magnetic and electric properties of $La_{0.70}Ba_{0.30}MnO_{3-\delta}$ ($0 \leq \delta \leq 0.30$) manganite with a perovskite structure. J. Exp. Theor. Phys. **95**, 308 (2002)
19. J. Rodriguez-Carvajal, Recent advances in magnetic structure determination by neutron powder diffraction. Phys. B **192**, 55 (1993)
20. A.K. Pramanik, A. Banerjee, Phase separation and the effect of quenched disorder in $Pr_{0.5}Sr_{0.5}MnO_3$. J. Phys. Condens. Matter **20**, 275207 (2008)
21. B. Christopher, A. Rao, V.C. Petwal, I.P. Verma, J. Dwivedi, W.J. Lin, Y.-K. Kuo, Influence of electron beam irradiation on electrical, structural, magnetic and thermal properties of $Pr_{0.8}Sr_{0.2}MnO_3$ manganites. Phys. B **502**, 119–131 (2016)
22. C. Martin, A. Maignan, M. Hervieu, B. Raveau, Magnetic phase diagrams of $L_{1-x}A_xMnO_3$ manganites ($L =$ Pr, Sm; $A =$ Ca, Sr). Phys. Rev. B **60**, 12191–12199 (1999)
23. M. Bourouina, A. Krichene, N. Chniba-Boudjada, M. Khitouni, W. Boujelben, Structural, magnetic and magnetocaloric properties of nanostructured $Pr_{0.5}Sr_{0.5}MnO_3$ manganite synthesized by mechanical alloying. Ceram. Int. **43**, 8139–8145 (2017)
24. L.E. Hueso, J. Rivas, F. Rivadulla, M.A. Lopez-Quintela, Tuning of the magnetocaloric effect in $La_{0.67}Ca_{0.33}MnO_{3-\delta}$ nanoparticles synthesized by sol–gel techniques. J. Appl. Phys. **86**, 3881 (1999)

25. N. Zhang, W. Ding, W. Zhong, W. Yang, Y. Du, J. Phys. Condens. Matter **9**, 4281 (1997)
26. J. Fontcuberta, B. Martinez, A. Seffar, S. Pinol, J.L. Garcia-Munoz, X. Obradors, Colossal magnetoresistance of ferromagnetic manganites: structural tuning and mechanisms. Phys. Rev. Lett. **76**, 1122–1125 (1996)
27. H.Y. Hwang, S.W. Cheong, P.G. Radaelli, M. Marezio, B. Batlogg, Lattice effects on the magnetoresistance in doped $LaMnO_3$. Phys. Rev. Lett. **75**, 914–917 (1995)
28. A. Jerbi, A. Krichene, N. Chniba-Boudjada, W. Boujelben, Magnetic and magnetocaloric study of manganite compounds $Pr_{0.5}A_{0.05}Sr_{0.45}MnO_3$ (A = Na and K) and composite. Phys. B **477**, 75–82 (2015)
29. A. Elghoul, A. Krichene, N. Chniba-Boudjada, W. Boujelben, Rare earth effect on structural, magnetic and magnetocaloric properties of $La_{0.75}Ln_{0.05}Sr_{0.2}MnO_3$ manganites. Ceram. Int. **44**, 12723–12730 (2018)
30. S.K. Banerjee, On a generalized approach to first and second order magnetic transitions. Phys. Lett. **12**, 16–17 (1964)
31. A. Arrott, J.E. Noakes, Approximate equation of state for nickel near its critical temperature. Phys. Rev. Lett. **19**, 786 (1967)
32. G. Huo, Y. Chang, X. Li, Z. Li, H. Li, Critical behavior and magnetocaloric effect in $La_{0.67}Sr_{0.33}MnO_{3.01}$ compounds. Solid State Sci. **87**, 15–20 (2019)
33. M.E. Fisher, The theory of equilibrium critical phenomena. Rep. Prog. Phys. **30**, 615 (1967)
34. B. Widom, Surface tension and molecular correlations near the critical point. J. Chem. Phys. **43**, 3892 (1965)
35. J.S. Kouvel, M.E. Fisher, Detailed magnetic behavior of nickel near its curie point. Phys. Rev. **136**, A1626 (1964)
36. Z.G. Zheng, X.C. Zhong, H.Y. Yu, V. Franco, Z.W. Liu, D.C. Zeng, The magnetocaloric effect and critical behavior in amorphous $Gd_{60}Co_{40-x}Mn_x$ alloys. J. Appl. Phys. **111**, 07A922 (2012)
37. J. Fan, L. Pi, L. Zhang, W. Tong, L. Ling, Investigation of critical behavior in $Pr_{0.55}Sr_{0.45}MnO_3$ by using the field dependence of magnetic entropy change. Appl. Phys. Lett. **98**, 072508–072514 (2011)
38. M. Baazaoui, S. Hcini, M. Boudard, S. Zemni, M. Oumezzine, Critical behavior near the ferromagnetic-paramagnetic phase transition temperature of $Pr_{0.67}Ba_{0.33}Mn_{1-x}Fe_xO_3$ ($x = 0$ and 0.05) manganite. J. Magn. Magn. Mater. **401**, 323–332 (2016)
39. J. Yang, Y.P. Lee, Critical behavior in Ti-doped manganites $LaMn_{1-x}Ti_xO_3$ ($0.05 \leqslant x \leqslant 0.2$). Appl. Phys. Lett. **91**, 142512–142525 (2007)
40. Z. Wang, J. Jiang, Magnetic entropy change in perovskite manganites $La_{0.7}A_{0.3}MnO_3$ $La_{0.7}A_{0.3}Mn_{0.9}Cr_{0.1}O_3$ (A = Sr, Ba, Pb) and Banerjee criteria on phase transition. Solid State Sci. **18**, 36–41 (2013)
41. A. Rostamnejadi, M. Venkatesan, P. Kameli, H. Salamati, J.M.D. Coey, Magnetocaloric effect in $La_{0.67}Sr_{0.33}MnO_3$ manganite above room temperature. J. Magn. Magn. Mater. **323**, 2214–2218 (2011)
42. M.-H. Phan, S.-C. Yu, N.H. Hur, Y.-H. Yeong, Large magnetocaloric effect in a $La_{0.7}Ca_{0.3}MnO_3$ single crystal. J. Appl. Phys. **96**, 1154 (2004)
43. M.H. Phan, H.X. Peng, S.C. Yu, D.T. Hanh, N.D. Tho, N. Chau, Large magnetocaloric effect in $Pr_{1-x}Pb_xMnO_3$ ($0.1 \leqslant x \leqslant 0.5$) Perovskites. J. Appl. Phys. **99**, 08Q108 (2006)
44. F.B. Jemaa, S.H. Mahmood, M. Ellouze, E.K. Hlil, F. Halouani, Structural, magnetic, magnetocaloric, and critical behavior of selected Ti-doped manganites. Ceram. Int. **41**, 8191–8202 (2015)
45. D.L. Rocco, R.A. Silva, A.M.G. Carvalho, A.A. Coelho, J.P. Andreeta, S. Gama, Magnetocaloric effect of $La_{0.8}Sr_{0.2}MnO_3$ compound under pressure. J. Appl. Phys. **97**, 10M317 (2005)
46. A. Nasri, E.K. Hlil, A.-F. Lehlooh, M. Ellouze, F. Elhalouani, Study of magnetic transition and magnetic entropy changes of $Pr_{0.6}Sr_{0.4}MnO_3$ and $Pr_{0.6}Sr_{0.4}Mn_{0.9}Fe_{0.1}O_3$ compounds. Eur. Phys. J. Plus **131**, 110 (2016)
47. H. Mbarek, R. M'nasri, W. Cheikhrouhou-Koubaa, A. Cheikhrouhou, Magnetocaloric effect near room temperature in $(1-y)La_{0.8}Ca_{0.05}K_{0.15}MnO_3/yLa_{0.8}K_{0.2}MnO_3$ composites. Phys. Status Solidi A **211**, 975 (2014)
48. V.K. Pecharsky, K.A. Gschneidner, A.O. Tsokol, Rep. Prog. Phys. **68**, 1479 (2005)
49. Y. Xu, M. Meier, P. Das, M.R. Koblischka, U. Hartmann, Perovskite manganites: potential materials for magnetic cooling at or near room temperature. Cryst. Eng. **5**, 383–389 (2002)
50. Q.Y. Dong, H.W. Zhang, J.R. Sun, B.G. Shen, V. Franco, A phenomenological fitting curve for the magnetocaloric effect of materials with a second-order phase transition. J. Appl. Phys. **103**, 116101–116101–116101–116103 (2008)

51. H. Oesterreicher, F.T. Parker, Magnetic cooling near Curie temperatures above 300 K. J. Appl. Phys. **55**, 4334 (1984)
52. V. Franco, J.S. Blázquez, A. Conde, The influence of Co addition on the magnetocaloric effect of Nanoperm-type amorphous alloys. Appl. Phys. Lett. **100**, 064307 (2006)
53. V. Franco, J.S. Blázquez, A. Conde, Field dependence of the magnetocaloric effect in materials with a second order phase transition: a master curve for the magnetic entropy change. Appl. Phys. Lett. **89**, 222512–222513 (2006)
54. V. Franco, A. Conde, Scaling laws for the magnetocaloric effect in second order phase transitions: from physics to applications for the characterization of materials. Int. J. Refrig. **33**, 465–473 (2010)
55. V. Franco, A. Conde, M.D. Kuz'min, J.M. Romero-Enrique, The magnetocaloric effect in materials with a second order phase transition: are T_C and T peak necessarily coincident? J. Appl. Phys. **105**, 917 (2009)

56. V. Franco, A. Conde, J.M. Romero-Enrique, J.S. Blazques, A universal curve for the magnetocaloric effect: an analysis based on scaling relations. J. Phys. Condens. Matter **20**, 285207 (2008)